Semiconductor Science and Technology

INVITED ARTICLE

Plasma-assisted molecular beam epitaxy of Al(Ga)N layers and quantum well structures for optically pumped mid-UV lasers on c-Al_2O_3

Semicond. Sci. Technol. **29** (2014) 084008 (10pp) doi:10.1088/0268-1242/29/8/084008

Invited Article

Plasma-assisted molecular beam epitaxy of Al(Ga)N layers and quantum well structures for optically pumped mid-UV lasers on c-Al_2O_3

S V Ivanov[1], D V Nechaev[1], A A Sitnikova[1], V V Ratnikov[1], M A Yagovkina[1], N V Rzheutskii[2], E V Lutsenko[2] and V N Jmerik[1]

[1] Ioffe Physical-Technical Institute, Polytekhnicheskaya 26, St. Petersburg 194021, Russia
[2] Stepanov Institute of Physics of NAS Belarus, Independence Ave. 68, Minsk 220072, Belarus

E-mail: ivan@beam.ioffe.ru

Received 17 January 2014, revised 4 April 2014
Accepted for publication 14 April 2014
Published 6 June 2014

Abstract

This paper reports on novel approaches developed for plasma-assisted molecular beam epitaxy of Al-rich AlGaN epilayers and quantum well heterostructures on c-sapphire, which allowed us to fabricate low-threshold optically-pumped separate confinement heterostructure lasers emitting in the mid-UV spectral range (258–290 nm) with the threshold power density below 600 kW cm^{-2}. The optimum buffer structure has been developed which provides lowering the near-surface threading dislocation density down to 1.5×10^8 and 3×10^9 cm^{-2} for screw and edge types, respectively, and improving the surface morphology (rms < 0.7 nm at the area of 3×3 μm^{-2}). It comprises the high-temperature (780 °C) migration enhanced epitaxy growth of a (30–70) nm thick AlN nucleation layer on c-Al_2O_3, followed by a 2 μm thick AlN buffer grown under the metal-rich conditions in the Al-flux modulation mode and containing several (up to 6) ultra-thin (~3 nm) GaN interlayers grown at N-rich conditions. Proper strain engineering in AlGaN single quantum well heterostructure grown atop of the AlN buffer layer enables one to preserve dominant TE polarization of both spontaneous and stimulated emission even at shortest obtained wavelength (258 nm). The threshold power density of stimulated emission as low as 150 kW cm^{-2} at 289 nm for a single quantum well laser structure has been demonstrated.

Keywords: AlGaN, molecular beam epitaxy, threading dislocations, optically-pumped laser, mid-UV range, polarization

(Some figures may appear in colour only in the online journal)

1. Introduction

The most essential problems of growing AlGaN heterostructures with moderate and high Al content ($x > 0.3$) for mid-ultraviolet (mid-UV) optoelectronic devices ($\lambda < 300$ nm), caused by absence of commercially available AlN and AlGaN bulk substrates, are (1) the lowering of the density of threading dislocations (TD) in the top active layers of the heterostructures below 10^9 cm^{-2} and (2) achieving the external quantum efficiency in quantum well (QW) heterostructure devices at least around 10% [1]. Meeting these severe requirements makes possible fabrication of both light-emitting and laser diodes (LEDs and LDs) for numerous applications in water–air disinfection systems, UV spectroscopy, covert optical communications etc. For the last decade, the most significant progress has been achieved in UV LEDs on c-sapphire demonstrating commercial devices in the 250–300 nm spectral range, possessing the quantum efficiency and output optical power values for a single LED chip of several per cent and tens of milliwatts, respectively [2]. The results for LDs are less impressive, showing the minimum lasing wavelength of 336 nm at room temperature under the pulse operation achieved by Yoshida *et al* in 2008 [3]. For the shorter wavelengths limited to 214 nm, laser and/or stimulated emission was obtained in QW structures, double heterostructures or bulk epilayers under the optical pumping only [4–7]. The best results with the lowest threshold power density of 84 kW cm^{-2} for lasing at $\lambda = 280.8$ nm have been recently shown by Xie *et al* [7] for AlGaN QW structures grown on bulk AlN substrates with the TD density as low as 10^3 cm^{-2}. Similarly, employing the bulk AlN substrates for growing UV LEDs allowed increasing their output power up to several tens of mW [8]. However, extremely large cost of the AlN substrates and their very limited stock stimulates numerous efforts to improve quality of AlGaN epitaxial structures on c-Al_2O_3 and other heterovalent substrates. The minimum threshold power density of optically-pumped AlGaN QW laser structures grown on c-Al_2O_3 by plasma-assisted molecular beam epitaxy (PA MBE), demonstrated to date, is noticeably higher—590 kW cm^{-2} (at $\lambda = 289$ nm) [9]. However, it is nearly half than that achieved by using metal-organic chemical vapor deposition (MOCVD) technique (~1 MW cm^{-2}) [5, 10, 11].

To reach the low threshold value in AlGaN structures grown by PA MBE on c-sapphire we have reduced TD density in the active QW region of the structures by adopting to MBE some techniques of TD filtering in Al(Ga)N buffer layers, developed earlier for MOCVD growth [12, 13]. The most significant effect on the TD lowering was achieved when two-dimensionally (2D) grown (1–2) μm thick AlN buffer layers incorporated multiple thin (~3 nm) compressively strained GaN layers [9] and/or were capped by AlGaN/AlN strained superlattices (SL) [9, 14]. The compressive stresses cause inclination of TD gliding from c-direction, which results in their efficient interaction and following annihilation [13, 15].

In addition, the atomically-smooth surface morphology of the AlN buffers is necessary to obtain, as it is inherited by the upper AlGaN cladding and waveguide layers and plays a crucial role in achieving stimulated and laser emission in AlGaN heterostructures. In relatively low-temperature PA MBE ($T_S = 700$–800 °C), the 2D growth mode of AlGaN can be achieved by using metal-rich growth conditions ensuring formation of thin (1–2 monolayers (ML)) surface metallic phase with enhanced adatoms mobility. To avoid metallic droplet formation on the surface of AlN buffer layers grown under the Al-rich conditions we elaborated the growth mode with periodically interrupted Al flux and continuous active nitrogen flux, controlled precisely by laser reflectometry (LR) technique, which ensured nearly continuous 2D growth of AlN [16]. Contrary to that, the droplet-free 2D growth of $Al_xGa_{1-x}N$ layers by PA MBE was usually controlled by accurate regulation of the excessive Ga flux at chosen growth temperature T_S, while x was determined by the F_{Al}/F_{N*} flux ratio [9]. High efficiency AlGaN QWs in the active region of the laser structures were fabricated by applying a sub-monolayer digital alloying (SDA) technique, with the effective QW composition being numerically defined by an AlGaN/GaN SL with sub-ML-thick GaN insertions [17]. This technique may offer rich opportunities in precisely grading the QW composition profile and modulating its surface morphology.

An additional challenge for reducing the threshold power density in Al-rich ($x > 0.25$) $Al_xGa_{1-x}N$-based QW laser structures is arranging a TE-polarization of the output radiation, which is a non-trivial task due to the crossover of heavy-hole and split-off-hole bands in AlGaN with increasing x, resulting in TM-polarization of photoluminescence (PL) [18, 19]. It appeared to be one of the reasons of relatively high threshold power densities (>1 MW cm^{-2}) demonstrated by Kawanishi *et al* [5, 20] in $Al_xGa_{1-x}N/Al_yGa_{1-y}N$ ($x = 0.67$, $y = 0.76$) multi-QW (MQW) structures emitting at 240.8 nm. Recently, Nortrup *et al* [21] have proposed to solve this problem by accumulating the strong compressive stress in the Al-rich AlGaN QWs, which suppresses the valence band crossover. Experimental confirmation of this idea was obtained in optically-pumped AlGaN laser structures grown pseudomorphically by MOCVD on bulk AlN substrates by Wunderer *et al* [6], which demonstrated TE-polarized 267 nm laser emission at strongly reduced threshold power density of 126 kW cm^{-2}. Analogous MQW structures grown on c-Al_2O_3 substrates by the same technique exhibited the spontaneous TM-polarized emission only [21].

This paper reports on recent developments of relatively low-temperature PA MBE growth of Al-rich AlGaN QW heterostructures on c-Al_2O_3 substrates, which result in demonstration of low-threshold stimulated and laser emission in the wavelength range 255–300 nm. The main issues to be discussed in detail are (i) further lowering of the TD density, which is achieved by optimization of initial growth stage of AlN nucleation layer on c-sapphire as well as proper choice of Al(Ga)N buffer layer structure and growth mode and (ii) realization of pseudomorphic growth conditions necessary for achieving TE-polarization of spontaneous and coherent mid-UV emission well below 290 nm.

2. Experimental details

2.1. PA MBE growth and sample details

All the structures were grown on standard c-Al_2O_3 substrates by using Compact21T (Riber SA) PA MBE setup equipped with a nitrogen plasma activator HD25 (Oxford Appl. Res.) The activator has a specially designed aperture plate that provides a linear control of the activated nitrogen flux from 0.25 to 0.65 monolayer s^{-1} (ML s^{-1}) by variation of the RF power in the (100–230) W range at the constant nitrogen mass flow of 5 sccm (growth pressure $3 \cdot 10^{-5}$ Torr) [9]. Typical nitrogen flux used during growth was kept constant at (0.4–0.5) ML s^{-1}, whereas Al and Ga fluxes varied in the ranges (0.2–0.6) ML s^{-1} and (0.3–0.8) ML s^{-1}, respectively, in dependence on the stoichiometric conditions used. The substrate temperature (T_S) was measured by an IR pyrometer calibrated by using the temperature dependence of GaN growth rate reduction at Ga- and N-polar surfaces [22].

AlN nucleation layers of 50–70 nm in thickness were grown by using the recently developed original technique of high-temperature (HT) ($T_S \sim 780\,°C$) migration enhanced epitaxy (MEE) which consists in alternate deposition of several (up to 4) MLs of Al and activated nitrogen N* [23]. We compare here the effect of such HT AlN nucleation layers on the structural quality of the whole AlGaN laser heterostructures to that achieved with a three-stage low-temperature (LT) ($T_S = 550\,°C$) AlN nucleation layers we employed earlier [9, 14].

The following 2 μm thick AlN buffer layer was grown at $T_S \sim 750$–$770\,°C$ under the metal-rich ($F_{Al}/F_{N*} \sim 1.4$) conditions with periodically interrupted Al flux and continuous N* flux, which ensured metal-free 2D surface morphology of the AlN buffer [16]. To suppress propagation of TDs through the buffer layers they involved several (up to 6) 3 nm thick GaN strained layers equally spaced by 130 or 260 nm. In some heterostructures, for the same purpose the $(AlGaN/AlN)_{20}$ strained SL with the average Al content $x \sim 0.8$ and period 10 nm was grown atop of the AlN buffer layer [9, 14].

The cladding and waveguide $Al_xGa_{1-x}N$ layers with x in the range 0.5–0.8 were grown also under the metal(Ga)-rich conditions at lower $T_S = 700$–$710\,°C$. To avoid Ga microdroplet occurrence we employed conventional MBE growth mode with precise control over the substrate temperature and the F_{Ga}/F_{N*} ratio which was always kept constant in between 1.1–1.3, while the Al flux controlled the Al content in the alloy (x) according to the expression $x = F_{Al}/F_{N*}$, as described in [9]. During $Al_xGa_{1-x}N$ growth the streaky RHEED pattern corresponding to a 2D growth mode was usually observed.

An $Al_xGa_{1-x}N$ single QW (SQW) was formed inside the (90–120) nm thick $Al_yGa_{1-y}N$ (y–x = 0.1) waveguide layer by the SDA technique [16], whereas its location was chosen to be asymmetric, the distance from the surface being approximately twice larger than that from the cladding interface, in accordance with calculations of the electro-magnetic wave maximum [9, 14]. In some heterostructures with high x in the SQW, the role of cladding layer was played by the AlN buffer.

2.2. Samples characterization

The PA MBE growth stoichiometry, growth rate and alloy composition were monitored *in situ* by a reflection high energy electron diffraction (RHEED) (former) and LR ($\lambda = 532$ nm). The epilayer and structure morphology, their internal design, and extended defects density and distribution were characterized *ex situ* by using scanning electron (SEM), atomic force (AFM) microscopies, as well as by transmission electron microscopy (TEM) (Philips EM-420). Besides, structural perfection and strain relaxation degree was estimated by employing x-ray diffractometry (XRD) studies of symmetric (0002) and skew-symmetric (10–15 tw) reflections, as well as reciprocal space mapping around asymmetric reflection (−1–124) (Bruker AXS D8 Discover). The latter technique was also used for defining layer composition (x) along with the *in situ* LR measurements of the individual growth rates from the calibrated F_{Al} and F_{N*} fluxes.

Optical properties of the heterostructures were studied by measuring spontaneous and stimulated photoluminescence (PL) excited by 4th and 5th harmonics of a Nd-YAG laser, respectively, the maximum excitation power density reaching 1 MW cm^{-2}. We used a transverse excitation geometry with the exciting beam being normal to the structure surface and PL being registered from the sample edge. Laser chips with cavity length below 1 mm were fabricated by cleaving from some heterostructures. They were excited by a stripe-focused laser beam with the stripe being normal to cavity mirrors [9].

3. Results and discussion

3.1. Initial growth stage on c-sapphire

Figure 1 demonstrates AFM images of the LT (figure 1(a)) and HT-MEE (figure 1(d)) AlN/c-Al_2O_3 nucleation layers (NLs), as well as cross-sectional TEM images (in two reflections, $\mathbf{g} = \{0002\}$ and $\mathbf{g} = \{01\text{–}10\}$) of 500 nm thick AlN buffer layers grown atop of these (30–70) nm thick NLs. A comparative analysis of the TEM images reveals the greater TD density at the initial AlN growth stage in case of LT NLs, which however drops significantly as T_S rises and a 3D growth mode (under N-rich conditions) is exchanged by a 2D one (Al-rich) (figures 1(b), (c)) (see [9] for detailed analysis). In the second case, the HT-MEE NL results in the much lower TD density at the very beginning of the AlN growth (figures 1(e), (f)).

Thus, both strategies are acceptable for reducing the TD density during the initial stage of PA MBE of AlN on c-sapphire. The LT NL provides generation of high density of TDs which facilitates them to interact with each other owing to changes of growth regimes (T_S and 3D-2D transition) which cause the inclination of the dislocation propagation direction with respect to c-axis (growth direction). This is followed by the efficient fusion of TDs and mutual annihilation through the dislocation loops formation [24]. In the case of HT-MEE NLs, the initial TD density is much lower, which can be explained by the lager nucleation grain diameter (compare figures 1(a) and (d)) and correspondingly the smaller length of inter-grain boundaries which are responsible for generation of screw and edge TDs [12]. The apparent twice larger roughness scale in figure 1(d), as compared to figure 1(a), is caused by larger inter-grain distance in the HT-MEE NL, while the in-plane grain surface is much flatter in this case. Probably, the HT-MEE NL serves also as the nanocolumnar buffer which can accommodate the strain induced by the following continuous AlN buffer layer thus reducing additionally generation of misfit dislocations. As can be seen from a comparison of figures 1(b) and (e), the HT-MEE nucleation results generally in lower screw TD density

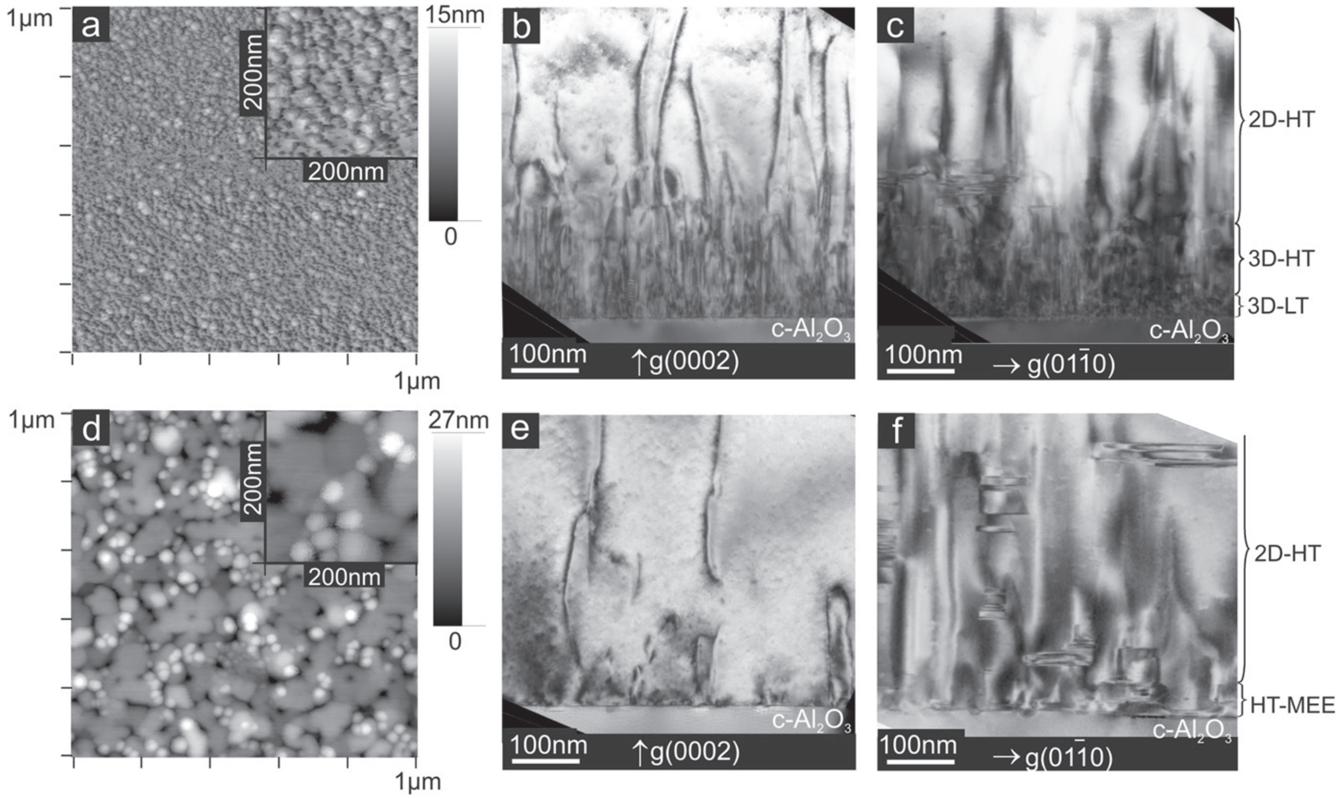

Figure 1. AFM surface images of (30–70) nm thick AlN nucleation layers grown on c-Al_2O_3 at low temperature in conventional MBE mode (a) and at high temperature in MEE mode (d). Cross-section TEM images taken at different reflexes (0002 and 01–10, exhibiting mostly screw and edge TDs, respectively) of 500 nm thick AlN buffer layers grown atop of the LT (b), (c) and HT-MEE (e), (f) nucleation layers. Mixed-type dislocations are detectable in TEM images at both reflexes.

in the following AlN buffer versus LT NLs. Moreover, one can observe formation of c-plane-oriented dislocation segments in both cases as soon as the 2D HT growth of AlN buffer starts. Origin of this effect of strong dislocation bending in the bulk AlN layer, which seems to suppress effectively propagation of TDs along the growth axis will be studied in detail elsewhere.

3.2. Suppression of TDs propagation in AlN buffer layers

We have found that the most efficient way to reduce the TD density in thick (2 μm) AlN buffer layers is incorporation of ultrathin (3–4 nm) GaN layers introducing strong compressive stress in the buffers, whose relaxation causes the inclination of TDs, accompanied by their interaction and annihilation. Growth of these multiple GaN insertions separated by 260 nm thick AlN layers was performed under slightly N-rich conditions ($F_{Ga}/F_{N^*} \sim 0.8$) which facilitate nucleation of gradually extending strained GaN micrograins on the AlN surface, rather than continuous 2D GaN layer usually formed under the Ga-rich conditions. The RHEED patterns used to exhibit occurrence of a mixed streaky-dotty picture during growth of the GaN insertions (2D–3D mode), which was immediately exchanged by a streaky one typical for the 2D mode as soon as AlN growth started under the Al-rich conditions.

Figure 2 illustrates the positive effect of the GaN insertions, which actually involves two mechanisms: (1) inclination of both types of TDs and (2) blocking of vertical propagation of TDs. The former mechanism which is more efficient at the bottom regions of the AlN buffer, where TDs' density is very high, enhances interaction between TDs, leading to formation of dislocation loops in the AlN layers in between the GaN insertions. The latter seems to work at each GaN insertion and even inside the AlN layers and results in 90° bending of TDs, followed by their propagation in the c-plane. This looks like TDs blocking at the TEM images.

The observed peculiarities of PA MBE growth of AlN buffer layers with the thin GaN insertions can be explained in the frame of phenomenological model of multi-stage relaxation of elastic stress in wurzite III-N heterostructures (including GaN/AlN), developed earlier in papers by Daudin's group [25, 26]. In accordance with this model, elastic stress relaxation at the GaN/AlN (0001) interface occurs mainly through gradual introduction of edge dislocations having Burgers vector $\mathbf{b} = 1/3\langle -12\text{-}10\rangle$ and gliding in lateral directions <10-10>. The generation rate of these edge dislocations depends in a complicated manner on growth kinetics of GaN nucleation layer composed of small platelets of several monolayers (MS) in height and several tens of nm in diameter. Most importantly, the generation rate slows down significantly in the case of 2D growth mode under Ga-rich conditions and accelerates when growth occurs in a 3D mode, i.e. under N-rich ones. Besides generation of new in-plane edge type dislocations, the stress relaxation in GaN may occur

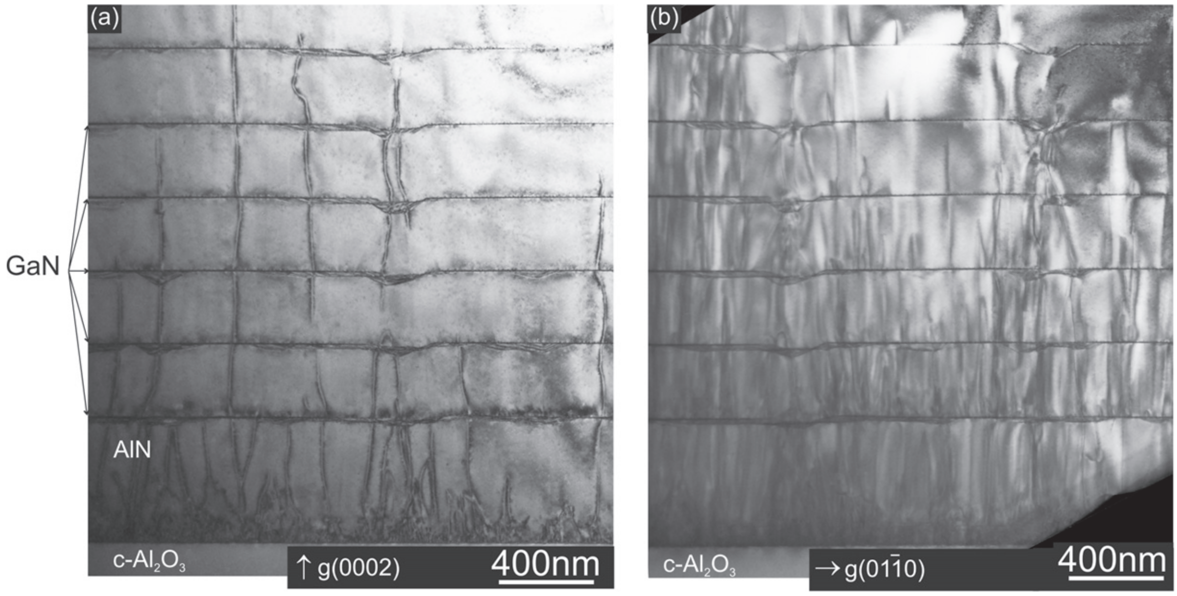

Figure 2. Cross-section TEM images at diffraction vectors $g = \{0002\}$ (revealing screw TDs) (a) and $g = \{01\text{–}10\}$ (revealing vertical edge TDs) (b) reflexes of thick 2D AlN buffer layer with six GaN ultrathin insertions grown under N-rich conditions. Mixed-type TDs are supposed to be displayed at both images.

by means of inclination of vertical edge TDs with the same Burgers vector ($\mathbf{b} = 1/3\langle -12\text{-}10\rangle$), which propagates in the AlN buffer layer from the AlN/c-Al_2O_3 interface [25].

Extrapolating these ideas to our case of several fast relaxing GaN 2D-3D interlayers incorporated in the AlN buffer possessing relatively high density of TDs, one can suppose that both mechanisms of stress relaxation are realized in the GaN insertions, the former being efficient in bending the vertical TDs into the basal plane (0001), which is observed in the TEM images. As follows from figure 2, the propagation of TDs is suppressed most efficiently at the bottom 3–4 GaN insertions where the TD density is the highest. One can also observe that high TD density disturbs the AlN growth front flatness, which is reflected in the roughness of the bottom GaN interlayers. Nevertheless, the inclination effects preserve in such places and perhaps are even enhanced, which results in significant reduction of TDs.

Figure 3 demonstrates the TEM cross-section and plan-view images of the top part of AlGaN SQW heterostructures grown on such a thick AlN/GaN buffer structure. The cross-section image (figure 3(a)) taken at diffraction vector $\mathbf{g} = \{0002\}$ exhibits TDs with a screw component, while the plan-view one allows estimation of the total TD density at the QW region as $\sim 6 \cdot 10^9\ \mathrm{cm}^{-2}$.

XRD studies of the SQW structure confirmed existence of residual compressive strain in the structure and revealed the ω-rocking curve FWHM values (w) for symmetric AlN (0002) and skew-symmetric (10–15 tw) reflexes as 470 and 1025 arcsec, respectively. The densities of screw (ρ_{sc}) and edge (ρ_e) TDs were estimated by using a standard equation for uniformly distributed TDs as $\rho = w^2/(4.35b^2)$, where b is the component of Burgers vector equal to 0.498 and 0.311 nm for the screw and edge TDs, respectively [27–29]. The XRD analysis results, $\rho_{sc} = 4.5 \times 10^8$ and $\rho_e = 6 \times 10^9\ \mathrm{cm}^{-2}$, show

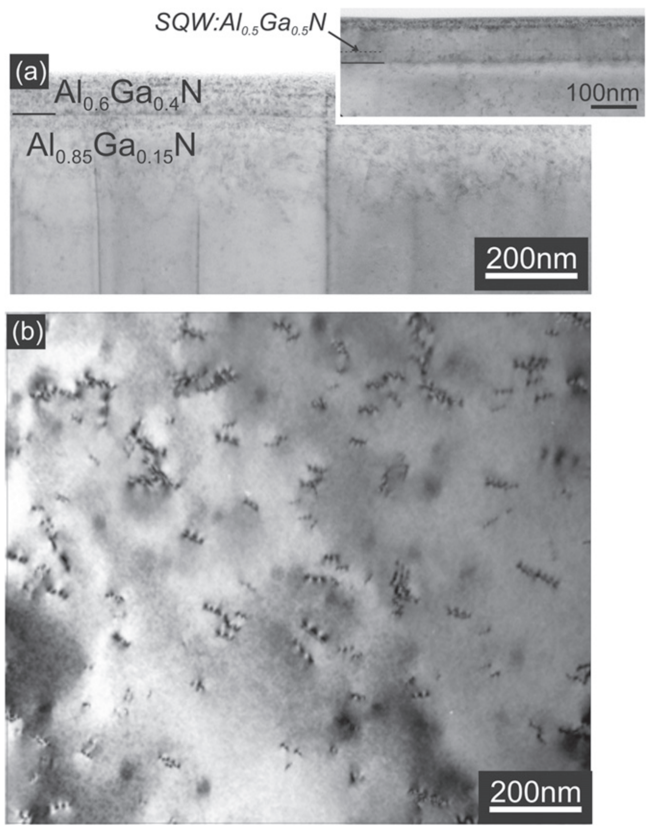

Figure 3. TEM cross-section $g = \{0002\}$ (a) and plan-view (b) images of AlGaN SQW structure grown atop of the thick AlN buffer with multiple 2D–3D GaN insertions.

good agreement with the estimations made from the TEM images. For comparison, the 2 μm thick AlN buffer layers grown on the HT-MEE NL under the same conditions but having no GaN insertion layers exhibited the appreciably

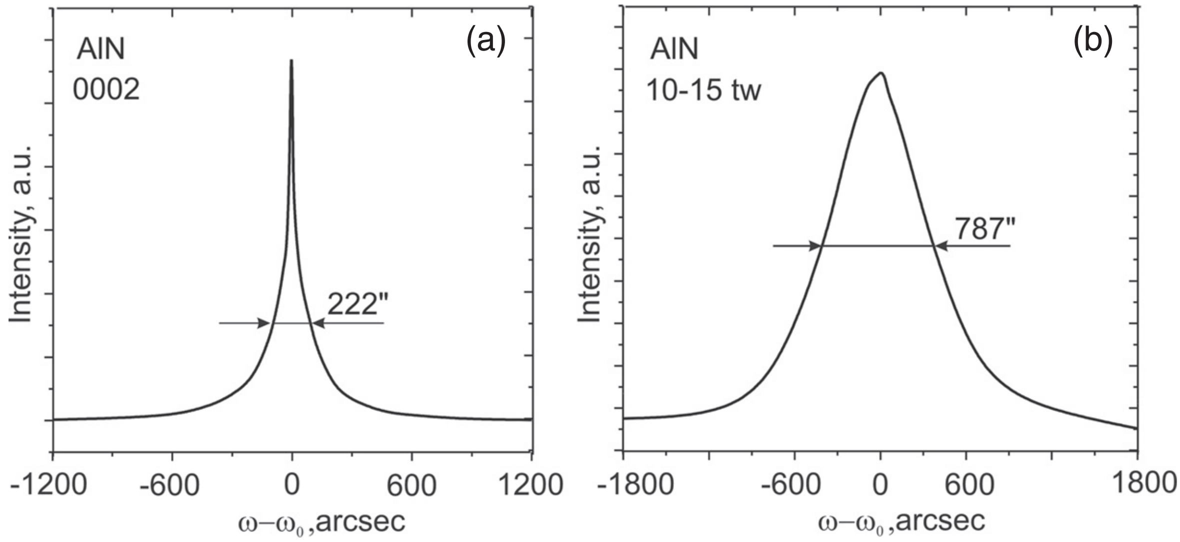

Figure 4. XRD rocking curves of AlN buffer layer in the SQW structure grown on c-sapphire with optimized AlN/GaN buffer design and growth conditions for symmetric (0002) (a) and skew-symmetric (10–15 tw) (b) reflexes.

wider ω-rocking curves for symmetric (0002) and skew-symmetric (10–15 tw) reflexes, namely 890 and 1320 arcsec.

It is worth noting that incorporation of the thin GaN insertions described above did not cause the usual generation of new TDs in AlN. Additional arguments in favor of employing the transient 2D–3D morphology of the GaN interlayers were obtained from the experiments with multiple 3.5 nm thick GaN insertions grown in a 2D mode under the Ga-rich conditions. Such GaN/AlN buffer structures with six 2D GaN insertions usually detached from the sapphire substrate, which evidences high residual compressive strain in the buffer structure caused by the slow generation rate of edge misfit dislocations in the 2D GaN insertions. Reducing the distance between 2D GaN interlayers from 260 to 130 nm resulted in detachment of the GaN/AlN buffer structure after growing of approximately twice thinner buffer layer. Slowing down the stress relaxation process in low-temperature metal-rich PA MBE of compressively strained GaN(0001), accompanied by strictly vertical propagation of TDs, was also observed previously in [30].

Some SQW structures contained strained AlGaN/AlN SL with average Al content of 80 mol% in between the AlN/GaN buffer structure and the AlGaN cladding layer. It also provided some lowering of the TD density by facilitating formation of dislocation loops, but the efficiency of this mechanism seems to be much less as compared with the effect of thin 2D–3D GaN insertions.

Figure 4 shows the XRD ω-rocking curves of a AlGaN SQW structure grown atop the optimized AlN buffer structure including an 80 nm thick HT-MEE AlN nucleation layer and a 2 μm thick AlN buffer layer grown under the Al-rich conditions with the six 3 nm thick GaN insertions possessing 2D–3D morphology. The symmetric AlN (0002) rocking curve (figure 4(a)) exhibited a complex structure composed of a very thin (FWHM = 32 arcsec) dynamic component and a wider background peak with the FWHM value of 270 arcsec. Such a rocking curve shape usually reflects the existence of at least two AlN sublayers with much better crystalline quality of the top one [31]. The estimated maximum density of screw TDs in AlN layers has been found to be as low as $\rho_{sc} = 1.5 \cdot 10^8\,cm^{-2}$. The skew-symmetric AlN(10–15 tw) peak (figure 4(b)) showed a larger FWHM value of 790 arcsec which however corresponds to the lowest reported values of the edge TD density ($\rho_e = 3 \cdot 10^9\,cm^{-2}$) for AlGaN structures grown by PA MBE on c-sapphire.

3.3. Pseudomorphic growth of AlGaN/AlN SQW heterostructures and valence band crossover

Figure 5 represents AFM surface images of a 100 nm thick $Al_{0.6}Ga_{0.4}N$ layer grown in a Ga-rich mode immediately on the optimized AlN buffer layer. According to the smaller scale image (figure 5(b)), the layer possesses a grain structure with the average lateral size of grains of about 1 μm. This agrees well with the minimum TD density estimated above from XRD of skew-symmetric reflection ($3 \cdot 10^9\,cm^{-2}$), especially if one takes into account that TD are distributed non-uniformly. On the surface of each grain a step-flow 2D growth mechanism is realized ensuring rms roughness of 0.42 and 0.7 nm over the areas 1×1 and $3\times3\,\mu m^2$, respectively. According to optical microscopy observations, most of the 2-inch wafer surface was free from metallic droplets. However, near the wafer edges having lower temperature during growth by $\Delta T \sim 10$–15 °C, formation of Ga microdroplets with a density of $\sim10^5\,cm^{-2}$ was usually observed, which requires elaboration of novel approaches to PA MBE growth of AlGaN layers, providing atomically-flat and droplet-free surface across the whole wafer. These approaches will be discussed in a separate paper.

Relatively thin (100–150 nm) $Al_xGa_{1-x}N$ layers ($x > 0.6$) grown by low-temperature PA MBE in a 2D growth mode (Ga-rich conditions) on the atomically flat AlN/c-Al_2O_3 buffer layer have also demonstrated practically no elastic stress relaxation. A typical XRD RSM diagram of the

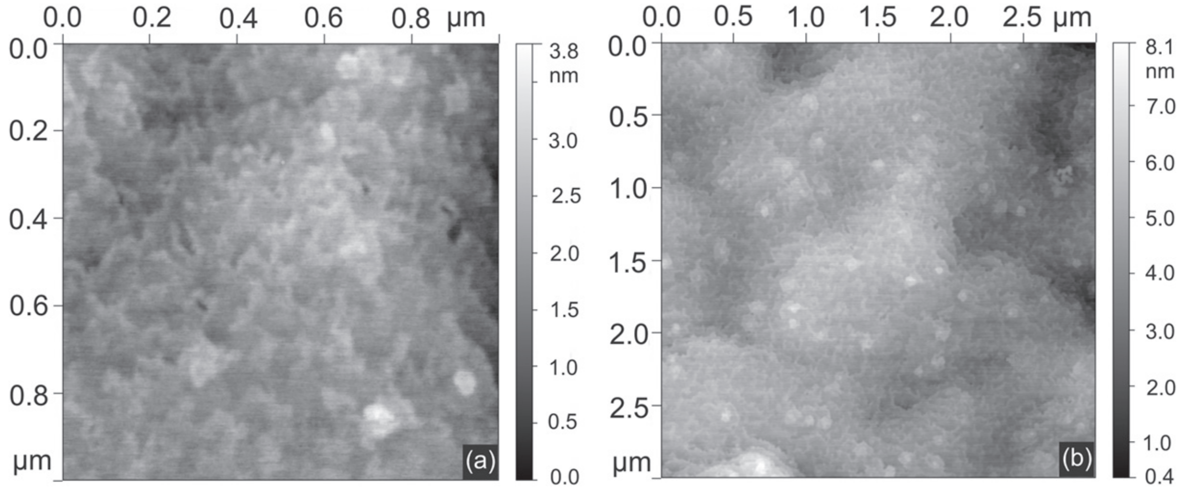

Figure 5. AFM images over the area ($1 \times 1\ \mu m^2$) (a) and ($3 \times 3\ \mu m^2$) (b) of 100 nm thick $Al_{0.6}Ga_{0.4}N$ layer grown atop of the optimized AlN/GaN buffer structure.

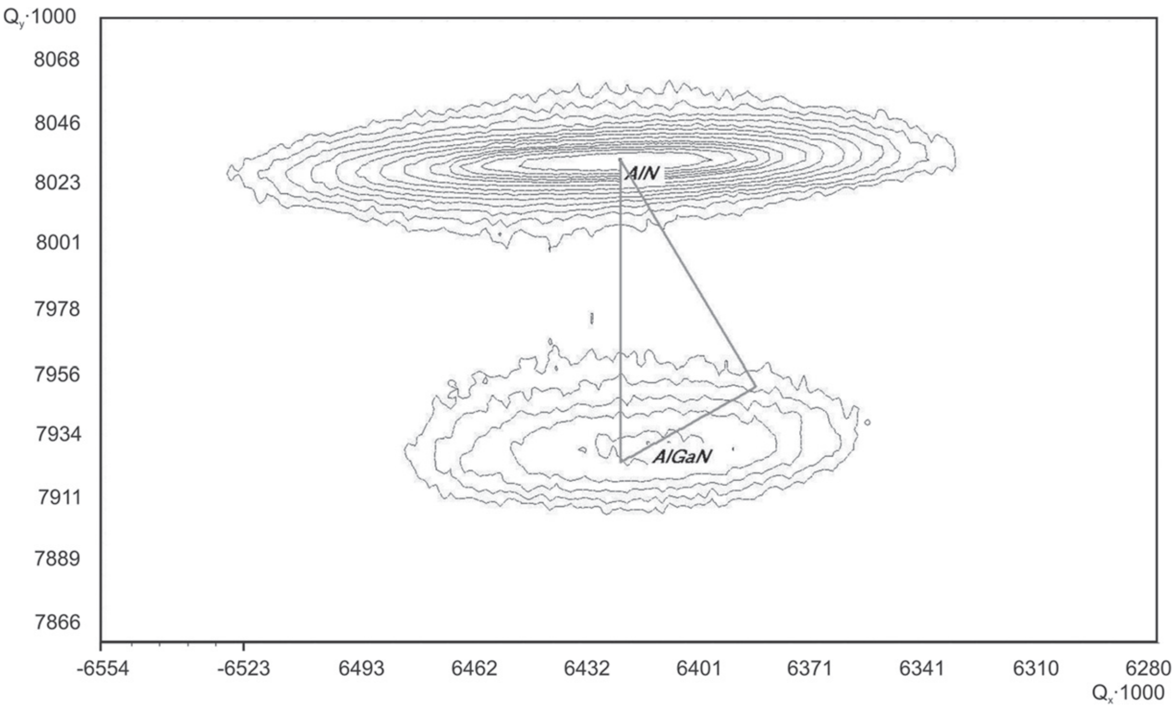

Figure 6. XRD reciprocal space mapping of a 100 nm-$Al_{0.78}Ga_{0.22}N$/2 mm-AlN/c-Al_2O_3 heterostructure grown by PA MBE under the metal-rich conditions in a 2D growth mode.

heterostructure comprising a 100 nm thick $Al_{0.78}Ga_{0.22}N$ layer and thick AlN buffer grown on c-sapphire, as was discussed in sections 3.1 and 3.2, is shown in figure 6. It reveals a rather small shift along the Q_x-axis of the AlGaN peak with respect to that of AlN (nominal level of the lateral strain is $\varepsilon_{xx} = -0.55\%$), which indicates that the stress relaxation degree in the top AlGaN layer does not exceed ∼10%.

This behavior can be explained by relatively small lattice mismatch between the top $Al_xGa_{1-x}N$ ($x > 0.6$) layer and the AlN buffer, strong kinetic limitations for TD emergence due to the 2D growth mechanism of the former, which provides the lowest surface density of nucleation sites for misfit dislocations formation, and the low-temperature ($T_S < 710$ °C) PA MBE conditions suppressing the dislocation gliding and inclination. As a result the AlGaN layers remain pseudomorphic.

However, according to XRD data, heterostructures containing either a relatively thick (200–700 nm) AlGaN cladding layer, or a compressively strained AlGaN/AlN SL, or both of them in between the AlN buffer and the top 100 nm thick AlGaN waveguide layer, usually exhibit rather large degree of stress relaxation in the waveguide layer up to 100%.

The difference in the heterostructure design and, as a consequence, in the stress relaxation degree resulted in an important observation of the change in polarization of the spontaneous emission from the $Al_xGa_{1-x}N$/AlN

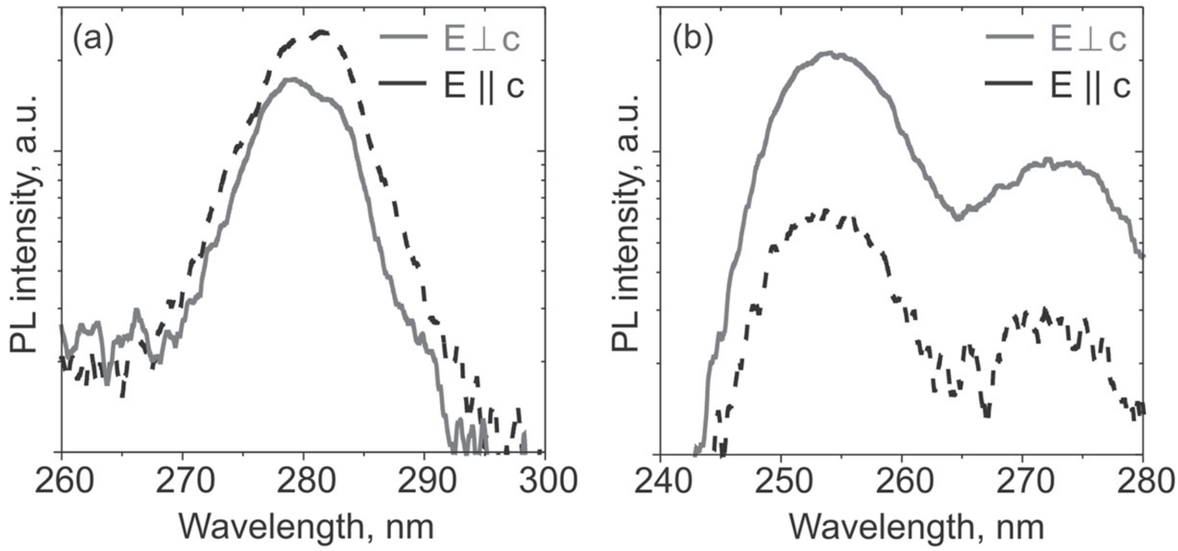

Figure 7. Spontaneous PL spectra of the AlGaN SQW structures with low (a) and high (b) residual compressive strain, measured from the cleaved structure edge under different polarizations: TE (***E***⊥c) and TM (***E***||c).

heterostructures. Figure 7(a) demonstrates that the PL intensity of TM polarized component (electric field vector is parallel to the *c*-axis) is higher than that of TE component (***E***⊥c) in the complex heterostructures comprising a 100 nm thick $Al_{0.5}Ga_{0.4}N$ waveguide layer with an embedded 2.5 nm thick $Al_{0.4}Ga_{0.6}N$ SQW, a 650 nm thick $Al_{0.75}Ga_{0.25}N$ cladding layer, and a $\{AlGaN/AlN\}_{40}$ SL with average $x = 0.85$ grown atop of the thick AlN buffer layer (TEM images of this structure are presented in figure 3). However, in the case of high residual compressive strain preserved in the top $Al_{0.78}Ga_{0.68}N$ waveguide layer containing a 2.5 nm thick $Al_{0.68}Ga_{0.32}N$ SQW, which was grown directly on the AlN buffer, the PL is dominated by TE-polarized component even at much shorter emission wavelength $\lambda = 250–260$ nm corresponding to the higher Al content in the QW (figure 7(b)).

This PL polarization behavior is related to the effect of residual compressive strain which is maximal in the latter heterostructure. It can reach the value $\varepsilon_{xx} \sim -0.7–0.8\%$ in the SQW, which corresponds to theoretical estimations of the compressive strain necessary for suppression of the valence band crossover in an AlGaN SQW even at the Al content above 70 mol.% [21]. As a result, spontaneous PL from the structures preserves TE polarization which is very important for efficient light extraction from mid-UV LEDs normally to c-plane as well as for achieving higher differential gain in the mid-UV laser cavity due to the higher reflectivity coefficient in the case of TE polarization of the cavity mode. This was the first demonstration of suppression of the valence band crossover in mid-UV AlGaN SQW structures grown on c-sapphire [32].

3.4. Stimulated emission from AlGaN SQW heterostructures

Figure 8(a) demonstrates an SEM cross-section image of optically-pumped SQW laser heterostructures grown on c-Al_2O_3 and designed using the whole set of TD filtering approaches developed by us so far, in particular, an HT-MEE NL, a 2.2 μm thick 2D AlN buffer layer with five thin 2D–3D Ga insertions, a 10 nm period $\{AlN/Al_{0.75}Ga_{0.25}N\}_{20}$ strained SL ($x_{av} = 0.9$), a 200 nm thick $Al_{0.75}Ga_{0.25}N$ cladding layer, and a 2.25 nm thick SDA $Al_{0.45}Ga_{0.55}N$ SQW embedded asymmetrically in a 120 nm thick $Al_{0.55}Ga_{0.45}N$ waveguide. The SQW composition and thickness were chosen to fit to the wavelength ~290 nm (still above the valence band crossover). The cleaved laser chip with a cavity length of 400 μm was pumped by a 4th harmonic of Nd:YAG laser ($\lambda = 266$ nm) at room temperature (RT). The edge PL spectra measured at different excitation power densities (figure 8(b)) exhibit occurrence of a narrow peak in the center of the PL band at 289 nm, whose intensity grows up non-linearly with the excitation while the line width decreases from 2.5 to 1.7 nm (at 300 kW cm^{-2}). The output optical power as a function of the excitation power density, shown in the inset of figure 8(b), demonstrates a pronounced kink at 150 kW cm^{-2} corresponding to the threshold power density of stimulated emission. Resolution of the detector used was not enough to resolve the longitudinal mode structure, whereas narrowing the far-field pattern of the output radiation was clearly observed above the threshold. This value is just twice higher than the record one achieved at $\lambda \sim 281$ nm in the AlGaN QW heterostructures grown on high quality bulk AlN substrates [7].

Similar behavior of edge PL spectra was observed in studies of a set of SQW laser structures with higher Al content in the QWs ($x_{QW} > 0.5$), the difference between Al content in the QW and barrier being kept constant and equal to $x_B – x_{QW} = 0.1$. The main difference of the laser structures from that considered above was the absence of AlGaN cladding layers and SL, i.e. the waveguide layers were grown immediately on the AlN buffer layer. According to results discussed in section 3.3, one can expect that the waveguide and QW remain strained with respect to the relaxed AlN buffer. The stimulated emission spectra of the structures, observed in

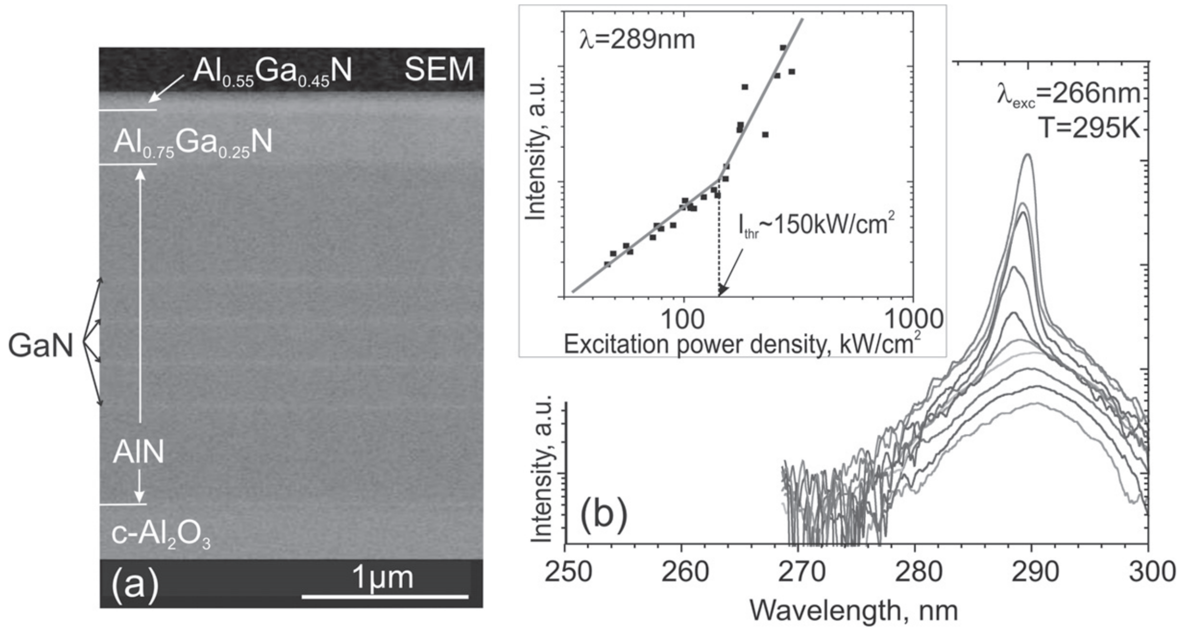

Figure 8. Cross-section SEM image (a) and edge PL spectra at different excitation power densities below and above the threshold (b) of the lowest threshold optically-pumped AlGaN SQW laser structure grown on c-Al_2O_3. Inset shows the output optical power versus excitation power density at RT.

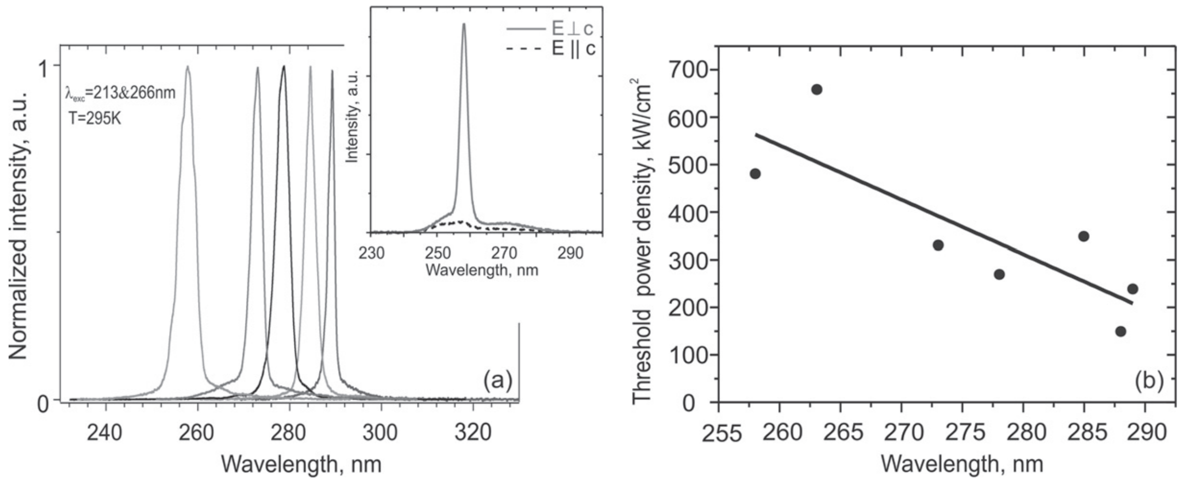

Figure 9. (a) Stimulated emission spectra of AlGaN SQW structures with Al content in SQW ranging from $x_{QW} = 0.5$ to 0.7. The inset demonstrates preferred TE polarization of stimulated emission at $\lambda = 258$ nm. (b) Threshold power densities of stimulated emission for these structures versus emission wavelength.

the spectral range $\lambda = 258$–289 nm, are summarized in figure 9(a). The inset in figure 9(a) shows polarized stimulated emission spectra of the shortest wavelength laser structure with $\lambda = 258$ nm, which exhibit the dominance of TE polarization ($\boldsymbol{E}\perp$c) even at $x_{QW} \sim 0.7$. This confirms the pseudomorphic nature of the waveguide and SQW, with the compressive stress in the QW above the critical value preventing the valence band crossover. The structures with the peak of stimulated emission at the longer wavelength demonstrated the similar intensity ratio between TE and TM components.

Figure 9(b) illustrates the dependence of the threshold power density of stimulated emission of the studied heterostructures on the emission wavelength. It exhibits clear raising from 150 till ~ 600 kW cm^{-2} as the QW composition x_{QW} increases from 0.5 to 0.7. This may be due to enhanced inhomogeneity of the barrier and QW layers with the increase of the Al content in the alloys, as confirmed by gradual widening of the stimulated emission peaks at shorter wavelength.

4. Conclusions

Summarizing, we have demonstrated the efficiency of several approaches applied in plasma-assisted MBE growth of AlN nucleation and buffer layers directly on c-Al_2O_3 for significantly improving structural quality and surface morphology of AlGaN SQW mid-UV laser heterostructures grown atop. Relatively high-temperature MEE growth of AlN nucleation layers and incorporation into the thick AlN buffer layer of stress-relaxed ultra-thin GaN interlayers grown in 2D–3D growth mode under the N-rich conditions have been shown to have main impacts on the suppression of generation of TDs at the AlN/c-Al_2O_3 interface and their efficient bending and inclination inside the AlN/GaN buffer structure. As a result the reduction of TD density down to 1.5×10^8 and 3×10^9 cm^{-2} for screw and edge types, respectively, has been achieved, which resulted in lowering the threshold power density of optically-pumped SQW separate confinement heterostructure lasers to 150 kW cm^{-2} at 289 nm. Preserving compressive stress in the AlGaN SQW structures pseudomorphically grown on strain-relaxed AlN buffer layers has enabled one to overcome valence band crossover in the QW and keep TE-polarization of both spontaneous and stimulated emission in the 258–290 nm range.

Acknowledgements

The authors are thankful to R V Zolotareva and P N Brunkov for assistance in TEM and AFM measurements. The work was supported in part by RFBR (♯♯13-02-12231-ofi-m and 12-02-00865) and BRFFR (♯F10R-164), and Programs of RAS and NASB.

References

[1] Kneissl M *et al* 2011 *Semicond. Sci. Technol.* **26** 014036
[2] Shatalov M *et al* 2012 *Appl. Phys. Express* **5** 082101
[3] Yoshida H, Yamashita Y, Kuwabara M and Kan H 2008 *Appl. Phys. Lett.* **93** 241106
[4] Shatalov M, Gaevski M, Adivarahan V and Khan A 2006 *Jpn. J. Appl. Phys.* **45** L1286
[5] Takano T, Narita Y, Horiuchi A and Kawanishi H 2004 *Appl. Phys. Lett.* **84** 3567
[6] Wunderer T, Chua C L, Yang Z, Northrup J E, Johnson N M, Garrett G A, Shen H and Wraback M 2011 *Appl. Phys. Express* **4** 092101
[7] Xie J *et al* 2013 *Appl. Phys. Lett.* **102** 171102
[8] Grandusky J R, Chen J, Gibb S R, Mendrick M C, Moe C G, Rodak L, Garrett G A, Wraback M and Schowalter L J 2013 *Appl. Phys. Express* **6** 032101
[9] Jmerik V N, Lutsenko E V and Ivanov S V 2013 *Phys. Status Solidi* A **210** 439
[10] Kneissl M, Yang Z, Teepe M, Knollenberg C, Schmidt O, Kiesel P and Johnson N M 2007 *J. Appl. Phys.* **101** 123103
[11] Mickevicius J, Jurkevicius J, Kazlauskas K, Zukauskas A, Tamulaitis G, Shur M S, Shatalov M, Yang J and Gaska R 2012 *Appl. Phys. Lett.* **100** 081902
[12] Bai J, Dudley M, Sun W H, Wang H M and Khan M A 2006 *Appl. Phys. Lett.* **88** 051903
[13] Jiang H, Egawa T, Hao M and Liu Y 2005 *Appl. Phys. Lett.* **87** 241911
[14] Jmerik V N, Mizerov A M, Sitnikova A A, Kop'ev P S, Ivanov S V, Lutsenko E V, Tarasuk N P, Rzheutskii N V and Yablonskii G P 2010 *Appl. Phys. Lett.* **96** 141112
[15] Fu Q M, Peng T, Mei F, Pan Y, Liao L and Liu C 2009 *J. Phys. D: Appl. Phys.* **42** 035311
[16] Jmerik V N, Mizerov A M, Nechaev D V, Aseev P A, Sitnikova A A, Troshkov S I, Kop'ev P S and Ivanov S V 2012 *J. Cryst. Growth* **354** 188
[17] Jmerik V N *et al* 2009 *J. Cryst. Growth* **311** 2080
[18] Leroux M *et al* 2002 *Phys. Stat. Sol.* B **234** 887
[19] Nam K B, Li J, Nakarmi M L, Lin J Y and Jiang H X 2004 *Appl. Phys. Lett.* **84** 5264
[20] Kawanishi H, Senuma M and Nukui T 2006 *Appl. Phys. Lett.* **89** 041126
[21] Northrup J E, Chua C L, Yang Z, Wunderer T, Kneissl M, Johnson N M and Kolbe T 2012 *Appl. Phys. Lett.* **100** 021101
[22] Mizerov A M, Jmerik V N, Kaibyshev V K, Komissarova T A, Masalov S A and Ivanov S V 2009 *Semiconductors* **43** 1058
[23] Nechaev D V, Aseev P A, Jmerik V N, Brunkov P N, Kuznetsova Y V, Sitnikova A A, Ratnikov V V and Ivanov S V 2013 *J. Cryst. Growth* **378** 319
[24] Cantu P, Wu F, Waltereit P, Keller S, Romanov A E, DenBaars S P and Speck J S 2005 *J. Appl. Phys.* **97** 103534
[25] Bourret A, Adelmann C, Daudin B, Rouvière J-L, Feuillet G and Mula G 2001 *Phys. Rev.* B **63** 245307
[26] Bellet-Amalric E, Adelmann C, Sarigiannidou E, Rouvière J L, Feuillet G, Monroy E and Daudin B 2004 *J. Appl. Phys.* **95** 1127
[27] Dunn C G and Koch E F 1957 *Acta Metall.* **5** 548
[28] Moram M A and Vickers M E 2009 *Rep. Prog. Phys.* **72** 036502
[29] Ratnikov V V, Kyutt R N, Smirnov A N, Yu Davydov V, Shcheglov M P, Malin T V and Zhuravlev K S 2013 *Crystallogr. Rep.* **58** 1023
[30] Cordier Y, Baron N, Chenot S, Vennéguès P, Tottereau O, Leroux M, Semond F and Massies J 2009 *J. Cryst. Growth* **311** 2002
[31] Faleev N, Lu H and Schaff W J 2007 *J. Appl. Phys.* **101** 093516
[32] Lutsenko E V, Rzheutskii N V, Pavlovskii V N, Yablonskii G P, Nechaev D V, Sitnikova A A, Ratnikov V V, Kuznetsova Ya V, Zhmerik V N and Ivanov S V 2013 *Phys. Sol. St.* **55** 2173